Experimental Research on Flexible Beam Modal Control

Bernd E. Schäfer* and Hans Holzach†
German Aerospace Research Establishment (DFVLR), Oberpfaffenhofen, Federal Republic of Germany

A hardware experiment has been developed to study the active vibration control (low-authority control) of a clamped-free flexible beam, where the design methodology is based on direct velocity feedback control. The objective of the experiment is to demonstrate and verify the dynamics and advanced control laws as applied to a structural element. Another important feature of the experiment is the feasibility of hardware realization, especially the dedicated noncontacting actuating and sensing method. Sensing is provided by a purely optical displacement sensor, while an electrodynamic force system provides the actuation. Experimental results are compared with numerical simulations of open- and closed-loop performance in both the colocated and noncolocated actuator/sensor positions. In most cases, good agreement is achieved between the experiments and theoretical predictions.

Nomenclature

A = cross section of beam
B = input matrix
b = width of beam; entries of matrix B
C = measurement matrix
c = eigenvector; entries of matrix C
D_0 = damping matrix
E = Young's modulus
E_D = dissipation energy
E_0 = total energy
F = external forces
f = natural frequency; vector of input forces
G = transfer function
g = acceleration due to gravity
h = beam thickness
I = momentum of inertia; identity matrix
K = feedback gain matrix
k = entries of matrix K
l = beam length
M = matrix of eigenvalue problem
m = beam mass; number of force actuators; entries of matrix M
N = truncation number
n = dimension of vector q
q = generalized coordinate vector
r = number of sensors
S = tensile force
s = transform variable
T = time constant
t = time
v = velocity
W = mode shape
w = beam deflection function
x = independent spatial variable
y = velocity vector
δ = Dirac delta function; Kronecker symbol
ζ = modal damping coefficient
η = efficiency factor
Λ = eigenvalue
λ = eigenvalue
ν = Poisson's ratio
ξ = nondimensional spatial variable
ρ = density
τ = nondimensional parameter including gravity
ϕ = comparison function
Ω = diagonal matrix containing eigenfrequencies
ω = natural circular frequency

Presented as Paper 84-1020 at the AIAA Dynamics Specialists Conference, Palm Springs, Calif., May 17-18, 1984; submitted July 19, 1984; revision received Jan. 3, 1985.

*Research Scientist, Section Spaceflight Dynamics.
†Member of Technical Staff, Section Spaceflight Dynamics.

Introduction

ADVANCED spacecraft systems are becoming increasingly complex as large lightweight structural elements become integral parts of the configuration. Furthermore, systems are now being considered that will no longer have a central rigid body. One essential characteristic of these space structures is their very low critical frequencies, which are falling within the attitude control system bandwidth. Hence, the question of vibration suppression by active modal control will become of fundamental importance. Although there are already a great variety of approaches to the theoretical control law,[1] the development of control experiments has grown much more slowly. Representatives of the first major attempts are described by Aubrun et al.[2] Interesting experimental studies of active vibration damping (low-authority control) have been performed on flexible beam structures having various supporting devices and using different types of sensors and actuators.[3-5] Controllers have been designed using full-state feedback and observer theory[3] or discrete Kalman filters.[4]

Controllers based on direct velocity feedback (described by Balas[6]) appear extremely simple compared to other approaches. Therefore, the objective of the present experiment is to demonstrate and verify this advanced approach on the basis of a new method for the optimal positioning of actuators and sensors on the structure to provide optimal feedback gains.[7] Further important features of the experiment are to demonstrate the feasibility of the dedicated noncontacting actuating and sensing devices.

Flexible Beam Configuration and Analysis

Test Setup

Since the main objective of the experiment has been directed toward the demonstration and verification of the dynamics and controller design, a simple structure with respect to dynamical modeling and its technical realization is required. For this purpose, the clamped-free homogeneous flexible beam hanging in the vertical direction (flexible pendulum) has been chosen as a suitable test structure. This con-

figuration can be regarded as being typical for a large variety of flexible elements (e.g., booms, antennae) in many spacecraft systems. The beam consists of nonmagnetic stainless steel (of the austenitic type) with a length of 2.90 m and a rectangular cross section of width 10 cm and thickness 1 mm; the total weight is 2.32 kg. A rigid, reinforced double-T girder weighing about 500 kg and mounted parallel to the beam at a distance of 5 cm serves as the supporting mechanism and is fixed to the wall (Fig. 1). At its upper end a clamp is mounted to support the flexible beam. An optical guide rail, as long as the beam, is attached along the supporting girder, serving as well-defined reference frame for carrying the actuating system. Moreover, the guide rail enables easy positioning of the actuator if other locations need to be investigated in the closed-loop tests.

Dynamic tests of the supporting mechanism have been performed in order to pinpoint any disturbances likely to occur by the interaction of the supporting beam with the flexible structure. The results show that minimum resonant frequencies at 56 and 82 Hz appeared to have no influence during the subsequent controller tests. In all experimental dynamic tests, a structural dynamics analyzer of type HP 5423A was used. It was a useful tool for studying and interpreting the results by means of time histories, frequency responses, and transfer functions.

Dynamic Model

For the controller design, a dynamic model of the flexible beam is required. The model is based on the Euler-Bernoulli theory that includes longitudinal loads due to gravity effects (Fig. 2). The partial differential equation of motion is

$$EIw^{IV} - (Sw')' + \rho A\ddot{w} = F(x,t) \tag{1}$$

together with the boundary conditions

$$w(0,t) = 0, \quad w'(0,t) = 0, \quad EIw''(l,t) = 0$$

$$EIw'''(l,t) - S(l)w'(l,t) = EIw'''(l,t) = 0 \tag{2}$$

where

$$S(x) = \rho Ag(l-x) \tag{3}$$

is the tensile force due to gravity.[8] At the clamped end, this force is equal to the beam's weight, while S is zero at the free end. The force distribution $F(x,t)$ comprises the applied control forces. These are ignored for the free vibration analysis to be considered now. A transverse harmonic motion of the form

$$w(x,t) = W(x)\sin\omega t \tag{4}$$

is assumed, where ω is the natural circular frequency and W the corresponding mode shape. With $\xi = x/l$, $\tau = \rho gAl^3/EI$, $\Lambda = \rho A\omega^2 l^4/EI$, Eq. (1) is replaced by

$$W^{IV}(\xi) - \tau[(1-\xi)W'(\xi)]' - \Lambda W(\xi) = 0 \tag{5}$$

No exact solutions are known for this boundary value problem. Therefore, an approximate approach for achieving a closed-form analytical solution is performed using Galerkin's method[9] with beam eigenfunctions ϕ_i (without gravity) as comparison functions in the Ritz expansion,

$$W(\xi) = \sum_{i=1}^{N} c_i\phi_i(\xi) \tag{6}$$

where the functions

$$\phi_i(\xi) = \cosh\lambda_i\xi - \cos\lambda_i\xi - \frac{\cosh\lambda_i + \cos\lambda_i}{\sinh\lambda_i + \sin\lambda_i}(\sinh\lambda_i\xi - \sin\lambda_i\xi) \tag{7}$$

are orthogonal and normalized with respect to

$$\int_0^1 \phi_k\phi_l d\xi = \delta_{kl}$$

and λ_i is the solution of $\cos\lambda_i\cosh\lambda_i = -1$. Inserting Eq. (6) in Eq. (5) finally leads to the special eigenvalue problem

$$(M - \Lambda I)c = 0 \tag{8}$$

where the symmetric and positive definite matrix M consists of the matrix elements

$$m_{kl} = \int_0^1 \phi_k[\phi_l^{IV} - \tau((1-\xi)\phi_l')']d\xi \tag{9}$$

Numerical results for the eigenvalue Λ and the corresponding eigenvector c have been obtained by standard methods with truncation number $N = 20$. A final design for a homogeneous flat beam yielded the geometrical and material parameters mentioned above. Because flat beams are plate-like structures, a correction on the assumption of pure bending is necessary[10]: transverse contraction will be restrained by additional transverse normal stresses that finally result simply in an increase of Young's modulus according to $E' = E \div (1-\nu^2)$. Moreover, in most practical cases, E is known with only poor accuracy, while the density ρ can be measured easily. Therefore, the modified wave velocity $\sqrt{E'/\rho}$ has been determined such that the five lowest natural frequencies agree very well with the corresponding experimental ones, giving finally a value of E that is about 20% lower than the expected one of $2 \cdot 10^{11}$ N/m^2.

Table 1 compares the theoretically and experimentally determined natural frequencies together with experimental modal damping parameters, where the experimental values of the first five modes have been determined by modal survey testing and the others by frequency response measurements using strain gages at the clamped end. The first column lists the theoretical natural frequencies of the same beam without gravity in order to exhibit the great impact of the gravity effects, especially at lower frequencies. The corresponding mode shapes are influenced very little by gravity when compared to the gravity-free modes not shown here. A graph of the first six mode shapes is shown in Fig. 3.

For experimental verification of the dynamic model, a model survey testing has been performed by means of the impact method. To identify the various mode shapes, the beam has been stimulated at different locations and the deflection measured by a displacement transducer. The transfer functions, generated by the spectral analyzer, yield the frequency and damping behavior (Table 1) together with the mode shapes. Good agreement with the theoretical predictions has been achieved. Additional information about the higher frequency range has been obtained by the strain gage mounted at the clamped end (Fig. 4).

Actuators and Sensors

The proper selection of the actuating and sensing system has been the focus of some effort. To achieve near-ideal performance (that is, to assess the performance of the control algorithms for the shape control of the beam), actuators and sensors having minimum interaction with the beam dynamics have been used. With this requirement, many sensor/ac-

tuator types were eliminated. Range and sensitivity were also restrictions. The sensors considered provide expected maximum vibration amplitudes of 10 mm and frequency ranges of about 100 Hz, since the designed controller will be based on the first five or six lowest modes and signals of higher frequency should be observable in order to account for possible instabilities. The expected force amplitudes range up to about 1 N. Highly accurate accelerometers of the magnetoresistive type, although being space applicable, have been discarded by their inherent physical effects: when mounted on the beam, they cannot distinguish between the desired horizontal acceleration and the undesired vertical component due to gravity, which might be of the same order of magnitude as the horizontal one, especially for low-frequency vibrations.

On this basis, noncontacting systems with laboratory-fixed references have been selected: a purely electro-optical displacement transducer (commercially available, of type Zimmer OHG 140) together with an in-house developed electrodynamic force actuator[11] provide for sensing and actuating (cf. Fig. 1). Since the underlying sensing and actuating methods are not in fact realizable in space (where there exists no rigid inertial support), this experiment does not focus on the complete problem of flexible spacecraft shape control, but rather on the limited problem of assessing controller performance and modeling fidelity when the influence of sensors and actuators can be almost ignored.

The actuator is of high resolution (<1%) with a range of 1.1 N and nonlinearity of 1% for a displacement range of ±12 mm. It consists of a permanent magnetic bar attached to the flexible beam that is free to move in a cylindrical laboratory-fixed electromagnetic coil (Fig. 5). The dimensions of coil and magnet have been determined such that the applied force is almost independent of their relative motion, resulting in an almost parabolic shape. To minimize errors in motion, a pair of coils is arranged at opposite sides of the structure. Driving these coils in parallel, the induced error in the axial motion will be essentially canceled. The small tilt

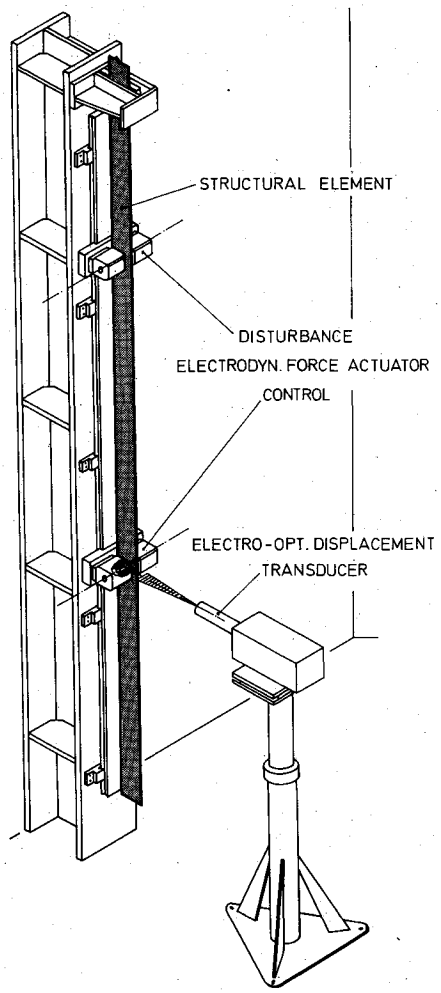

Fig. 1 Flexible beam test setup.

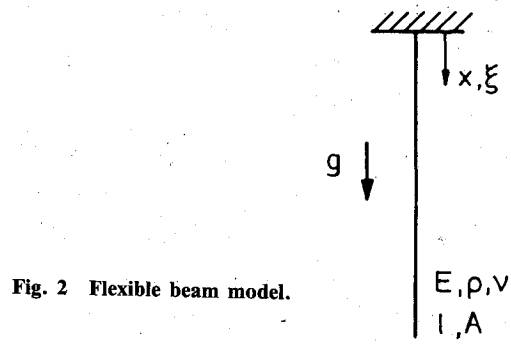

Fig. 2 Flexible beam model.

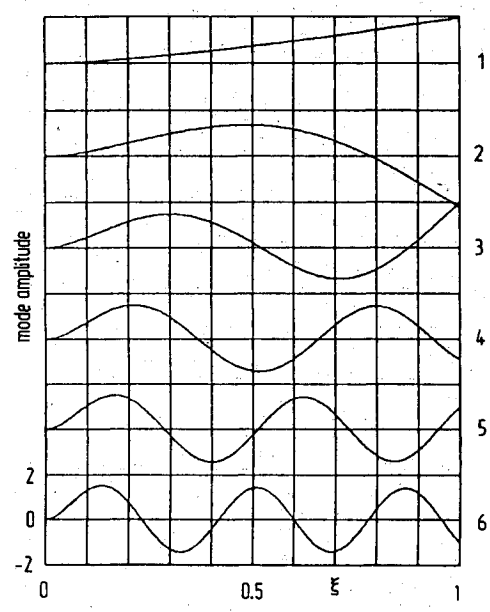

Fig. 3 Six lowest mode shapes.

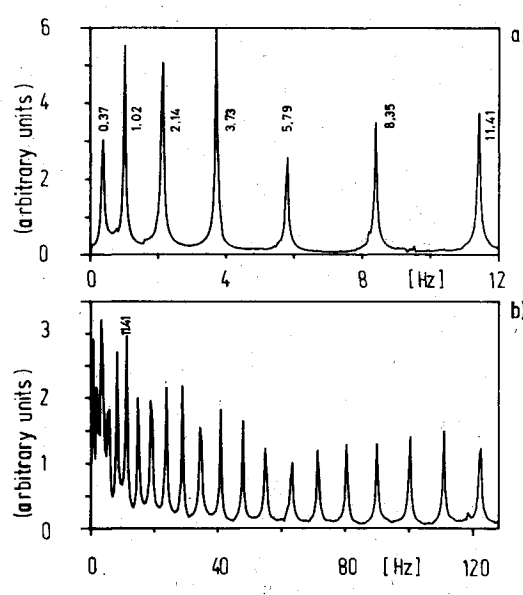

Fig. 4 Transfer functions showing a) the lowest 7 (0.05 Hz resolution) and b) the lowest 22 (0.8 Hz resolution) natural frequencies.

angle of the vibrating flexible beam proved to have no remarkable influence upon system nonlinearities. Additional mass concentrations due to the mounted pair of cylindrical, rare earth magnetic bars are negligible, considering a weight of 25 g for each bar having a length of 4 cm and diameter of 1 cm. This has been shown experimentally by frequency analyses when varying the locations of the bar along the beam in discrete spatial steps. The observed frequency variation remained below 3%.

The electro-optical displacement transducer requires an illuminated beam target as reference point for sensing, which is provided by the beam-mounted magnetic bar vibrating with the structure. The transducer then is placed perpendicular to the plane of the beam vibrations at a distance of 30 cm to the beam's symmetry axis and the target is projected on the photocathode of the transducer's image converter. Detection units installed on the transducer, driven by triangular signals derived from a generator, then cause pulses at the output of the built-in electron multiplier, which are proportional to the target deflection. With very low noise levels, the transducer has an excellent resolution of about 0.01% full scale in a range of about 10 mm. The range easily can be varied by changing the imaging optics. Nonlinearity is below 0.01% and frequency range extends to 1 kHz.

The actuating/sensing system provides for an almost ideal realization of colocated actuator/sensor positioning since the beam-mounted magnetic bar vibrating with the structure serves as the reference point for sensing (cf. Fig. 1). Noncolocated actuator/sensor positioning has been realized by a similar configuration fixing a small black-and-white edge sheet at the specified position.

The controller requires velocity information for the feedback that is extracted from the optical displacement signal by a differentiation procedure. Since no other controller algorithms have been proposed, it was preferred to realize differentiation by an analog technique rather than by a data processing system. The analog differentiator is characterized by a transfer function of type $G(s)=T_1 s/(1+T_2 s)$, with time constants $T_1=0.01$ s and $T_2=0.0015$ s, yielding a roll-off frequency of 667 rad/s.

Bandwidth limitation of the sensor signal is necessary to avoid the saturation effects of the differentiation loop. During the tests, no instability has been observed due to phase shifts in sensor signal and differentiation circuit.

Controller Design

The objective of the controller to be designed is to increase damping of the structure by direct velocity feedback. The flexible beam dynamics with m point-force actuators

$$F(x,t)=\sum_{i=1}^{m} f_i(t)\cdot\delta(x-x_i) \tag{10}$$

is described by Eq. (1). The velocities are measured by r point sensors,

$$y_j(t)=\dot{w}(x_j,t), \quad j=1,\ldots,r \tag{11}$$

The solution of Eq. (1) can be expanded in the mode shapes given by Eq. (6),

$$w(x,t)=\sum_{k=1}^{n} W_k(x)q_k(t) \tag{12}$$

where the generalized coordinate vector $q=[q_1,\ldots,q_n]^T$ satisfies the modal state space equation (with added modal damping assumed)

$$\ddot{q}+D_0\dot{q}+\Omega q=\frac{1}{m}Bf \tag{13}$$

where $\Omega=\mathrm{diag}(\omega_k^2)$, $D_0=\mathrm{diag}(2\zeta_k\omega_k)$, B is a $n\times m$ matrix with entries $b_{ki}=W_k(x_i)$, $m=\rho Al$, and the vector of input forces is $f=[f_1,\ldots,f_m]^T$. The sensor equation (11) then becomes

$$y(t)=C\dot{q}(t) \tag{14}$$

with $y=[y_1,\ldots,y_r(t)]^T$ and C is a $r\times n$ matrix with entries $c_{jk}=W_k(x_j)$. For direct velocity feedback, the control law is obtained by

$$f(t)=-Ky(t) \tag{15}$$

where K is the $m\times r$ gain matrix. Then the dynamical behavior of the closed-loop system is described by

$$\ddot{q}+\left(D_0+\frac{1}{m}BKC\right)\dot{q}+\Omega q=0 \tag{16}$$

In case of colocated sensors and actuators (i.e., $m=r$ and $B^T=C$), K non-negative definite, and no zero frequencies, it can be shown[6] that Eq. (16) has asymptotically stable solutions if $\zeta>0$ (even if the truncated residual modes are implemented), which is fulfilled since internal damping is present in all flexible structures. In case of dislocation, instability may occur as soon as truncated residual modes having nodal points between the actuator and sensor positions (spillover effect) are implemented in the model.

The important problem of suitably positioning actuators and sensors has been treated by Schulz and Heimbold[7] who presented a new method for an integral determination of actuator/sensor positions (included in B and C) and feedback

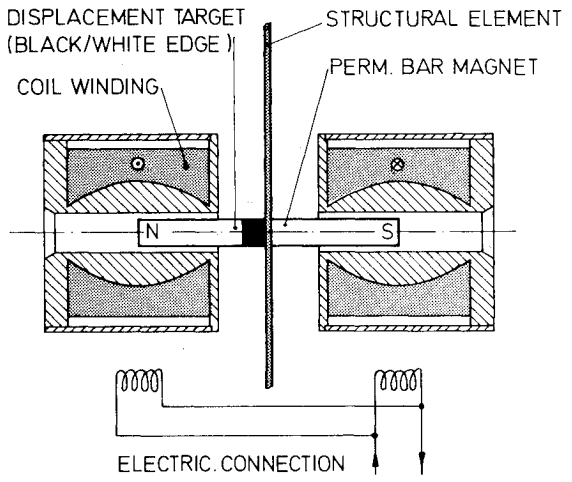

Fig. 5 Electrodynamical force actuating system.

Table 1 Natural frequencies and modal damping parameters for beam

j	Natural frequencies f_j, Hz: Theory (without g)	Theory (with g)	Exp. (with g)	Exp. modal damping, %
1	0.09	0.37	0.37	0.30
2	0.56	1.02	1.02	0.24
3	1.58	2.14	2.14	0.16
4	3.09	3.73	3.72	0.14
5	5.12	5.79	5.80	0.13
6	7.64	8.35	8.39	0.12
7	10.67	11.41	11.41	0.1
8	14.21	14.96	15.1	<0.1
9	18.25	19.01	19.2	<0.1
10	22.80	23.57	23.9	<0.1

gains (matrix K) for the system of Eq. (16). The method is based on the maximization of the dissipated energy caused by the control action,

$$E_D = -\int_0^\infty \dot{q}^T \cdot BKC \cdot \dot{q}\, dt \tag{17}$$

which represents an optimization criterion guided only by physical considerations. Additionally, constraints (upper bounds of ± 50 N·s/m) have been imposed on the feedback matrix K because of restricted maximum control forces exerted by real actuators.

Initial disturbance forces is realized by an impulsive point force acting on the beam and producing an initial velocity v_0 at the point of impact. The energy distribution among the modes of the total energy E_0 stored in the flexible structure is very strongly influenced by the position of the originating disturbance, and hence it influences the optimal actuator/sensor positions and the feedback gains. In order to excite many of the lower structural modes, the initial force has been applied near the clamped end at $\xi = 0.2$ rather than at the free end (in order to avoid an ideal disturbance compensation at the free end). To comply with realistic conditions, the force impact has been chosen as to achieve $v_0 = 30$ mm/s to give a maximum amplitude of about 5 mm at the free end.

The design model accounts for the lowest five vibration modes. An evaluation model including higher modes has been considered with $n = 10$ in order to investigate the stability of the residual five modes on the basis of the design model. The natural frequencies and mode shapes were determined analytically together with the experimentally obtained structural damping factors entered into the controller design. Furthermore, an efficiency factor $\eta = E_D/E_0$, giving the fraction of the total energy dissipated due to control action, has been considered in order to judge the optimal solutions.

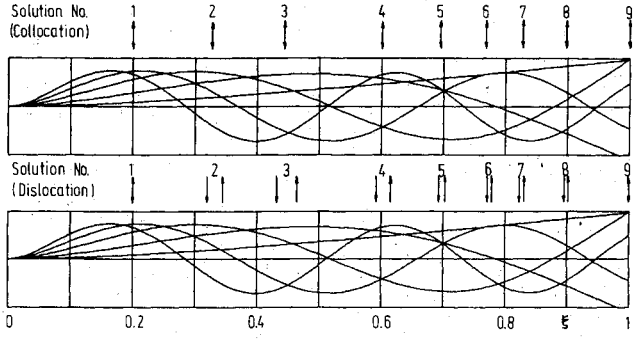

Fig. 6 Optimized actuator/sensor positions for colocated and dislocated configurations (↑actuator sensor) based on a five-mode controller.

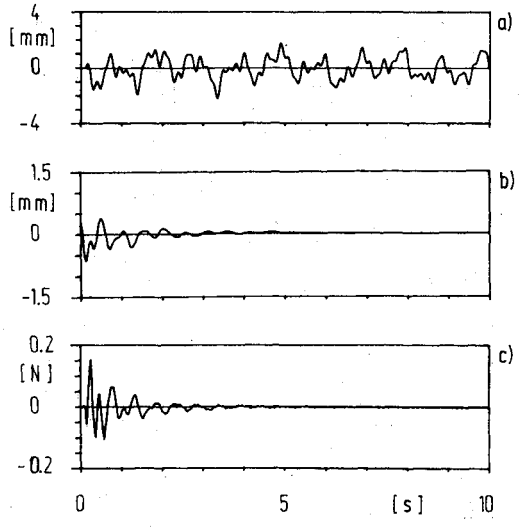

Fig. 7 Experimental time histories at $\xi = 0.602$: a) open- and b) closed-loop displacement; c) control force.

Experimental and Numerical Results

An inherent basic problem of the optimization procedures used is that no global optimum could be found. The optimal parameters achieved depend upon their initial values. Hence, several optima may result that are regarded as being only locally optimal. An important feature of the experimental investigations therefore is to judge the closed-loop behavior for different optima. The studies are performed for a one actuator/sensor configuration for both colocated and noncolocated positions. Furthermore, to get a first insight experimentally into the treatment of multiple actuator/sensor locations, a configuration of two actuators and two sensors is realized. Here, the study is confined to colocated positions in order to avoid excessive parameter combinations for the positions.

For verification of the designed control law, the variation of the closed-loop system eigenvalues with respect to the corresponding open-loop values has been determined by means of a transfer function measured between the force impact input as $\xi = 0.2$ and the displacement output at the optimized sensor position. In case of highly damped systems, excitation by white noise has been preferred rather than by impact in order to put more energy into the structure.

The disturbance impulse has been realized experimentally by a separate electrodynamic actuator system. A further displacement sensor has been positioned at $\xi = 0.2$ to determine the initial velocity v_0 by subsequent analog differentiation of the sensor signal. The pulse height and width can be adjusted to defined initial conditions to comply with the desired value of v_0, yielding 0.15 N and 50 ms. The adjustment of v_0 is necessary for comparison of experimentally and numerically obtained time histories.

One Actuator/One Sensor (Colocation)

Nine locally optimal positions have been obtained, each lying between adjacent zero crossings of the mode shapes as

Table 2 Optimal parameters of one actuator/sensor configuration (colocated)

No.	ξ	k_{11}, Ns/m	η, %
1	0.2	50.0	99.4
2	0.329	15.43	88.4
3	0.445	14.29	93.1
4	0.602	13.30	92.2
5	0.699	12.33	84.1
6	0.774	10.05	85.7
7	0.830	10.33	91.3
8	0.900	10.60	76.5
9	1.0	3.96	79.1

Table 3 Closed-loop eigenvalues for optimized position at $\xi = 0.602$ of one actuator/sensor configuration (colocated)

Model No.	Frequency, Hz		Modal damping, %	
	Exp.	Num	Exp.	Num.
1	–	–	–	100.0
2	0.7	0.70	10.2	15.0
3	1.9	1.96	8.3	7.6
4	3.5	3.57	7.6	7.7
5	4.9	5.33	12.7	11.5
6	8.3	8.35	1.1	0.5

presented in Fig. 6. The feedback gain matrix now consists of only a single element k_{11}. Table 2 lists the optimized position, feedback gain k_{11}, and the corresponding efficiency factor η for the various optima. Striking position 1 can be expected to be due to an ideal disturbance compensation that causes the optimizer to move the actuator at the position of the originating disturbance, thus giving an extremely high gain identical to the upper bound constraint in the present case. Positions 2-8 show gains of comparative size but with quite different efficiency factors. This means that high gains do not automatically yield low decay time constants in order to damp the vibrations quickly, since the damping behavior is obviously influenced strongly by the modal amplitude at the actuator/sensor position. This behavior is evident for position 5, where the sizes of mode shapes 2, 4, and 5 is much lower than those of modes 1 and 3. In contrast, at the free end a very low gain factor is obtained, mainly due to the large deflection of the mode shapes there.

Figures 7 and 8 present open- and closed-loop time histories for two optimized positions: one at $\xi = 0.602$ (Fig. 7 shows displacement and applied control force) and one at the free end (Fig. 8 shows displacement only compared to the numerical results). Experimentally determined transfer functions for both positions are presented in Fig. 9 for open- and closed-loop systems. The resulting eigenvalues (i.e., shifted resonant frequencies and modal damping factors) are listed in Tables 3 and 4 together with the calculated values for the first six modes. Although quite good agreement is indicated, proper eigenvalue determination of the lower frequency modes often appeared difficult due to high damping rates, which is most evident at $\xi = 0.602$. In accordance with theoretical predictions, no unstable modes could be observed during these tests.

One Actuator/One Sensor (Dislocation)

Again, nine locally optimal positions are obtained, where the initial values for both actuator and sensor have been chosen so as to lie between adjacent zero crossings of the five lowest modes. The results are presented in Fig. 6 and in Table 5, indicating a very close spacing between the actuator and sensor positions. Obviously, in order to avoid zero crossings between adjacent actuator and sensor positions, this spacing becomes closer if more modes are implemented in the design model, thus approaching the colocated case. The energy extracted by the actuator and the feedback gains are only insignificantly higher than in the colocated case. Moreover, it turns out that in the colocated case the actuator/sensor position always lies about in the middle of the corresponding dislocated positions.

Spillover is predicted in cases 3 and 4 when implementing the residual five modes ($n = 10$ now) in the evaluation model, caused by the nodal points of higher mode shapes between the actuator and sensor positions. For experimental demonstration of spillover, only position 4 will be investigated. Here, the sensor and actuator are separated by a distance of only 6.7 cm. The closed-loop time history of the displacement at sensor location is presented in Fig. 10a and shows that the lower vibration modes are damped out, but mode 6 with a frequency of 8.4 Hz and a nodal point at $\xi = 0.6$ (cf. Fig. 3) is excited very strongly.

To avoid spillover in this case, an extension of the controller design has been attempted on the basis of a six-mode design model, thus including the unstable vibration mode. Now the actuator and sensor move closer in order to exclude the critical zero crossing, yielding ξ (actuator) $= 0.5692$ and ξ (sensor) $= 0.5787$, $k_{11} = 12.85$ N·s/m, and $\eta = 96.6\%$. Figure 10b indicates stability of the closed-loop system. The very close distance of 2.7 cm appears almost colocated and it may be conjectured that in the colocated case the optimal positions will be somewhere between these two dislocated positions. The subsequent controller design verifies this suggestion, yielding optimal parameters of $\xi = 0.5741$, $k_{11} = 12.53$ N·s/m, and $\eta = 96.5\%$, which are not much different from the dislocated case.

Two Actuators/Two Sensors (Colocation)

The gain matrix K now comprises four elements to be optimized. Different choice of a specific form of K has been followed in the design, depending upon the choice of number

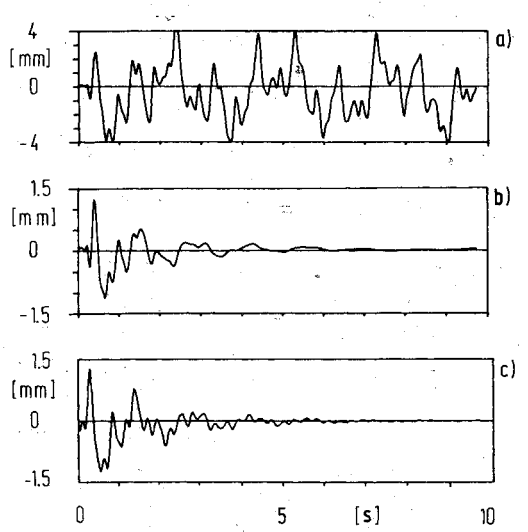

Fig. 8 Time histories of displacement at $\xi = 1.0$: experimental a) open- and b) closed-loop displacement; c) numerical closed loop.

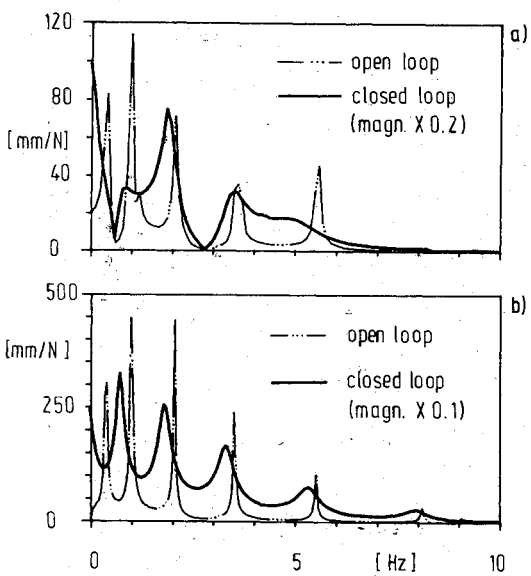

Fig. 9 Experimental open- and closed-loop transfer functions for optimized colocated positions: a) $\xi = 0.602$ and b) $\xi = 1.0$.

Table 4 Closed-loop eigenvalues for optimized position at $\xi = 1.0$ of one actuator/sensor configuration (colocated)

Mode No.	Frequency, Hz		Modal damping, %	
	Exp.	Num.	Exp.	Num.
1	–	–	–	100.0
2	0.7	0.73	11.9	12.1
3	1.8	1.88	7.3	7.6
4	3.3	3.67	5.4	1.9
5	5.3	5.73	4.6	2.1
6	8.0	8.30	3.3	1.8

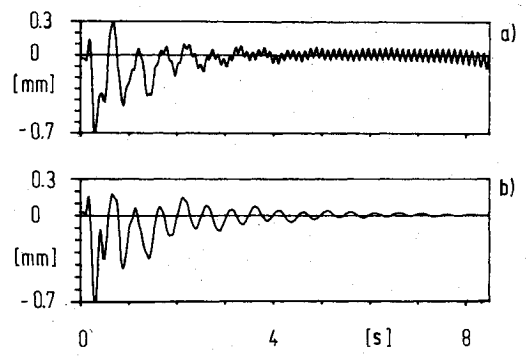

Fig. 10 Experimental closed-loop time histories of displacement for two controllers (dislocation): a) instable sixth mode, ξ(sensor) = 0.614; b) stable behavior, ξ(sensor) = 0.579.

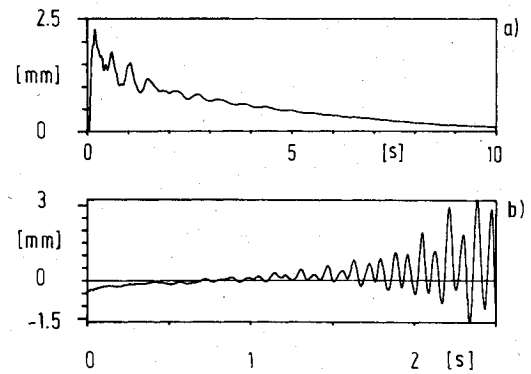

Fig. 11 Experimental closed-loop time histories of displacement at $\xi = 1.0$ for two actuators/two sensors controller: a) global feedback, b) axial feedback (here increasing oscillation from equilibrium position).

of sensor signals to be fed back. This has been realized numerically by equating to zero the corresponding matrix elements of K. The purpose of choosing different feedback strategies is to investigate the possibility of meeting controller performance requirements with just a few sensors and actuators. To be convenient, the actuator and sensor positions have been taken from the optimized one sensor/actuator case at $\xi = 0.602$ and 1.0 rather than optimizing these positions here. Three different feedback schemes have been considered for which the gains have been optimized, giving the following results:

$$1)\ K = \begin{pmatrix} 7.53 & -0.95 \\ 8.38 & 3.31 \end{pmatrix} \text{N·s/m},\ \eta = 94.7\%,$$

i.e., all sensor signals are fed back to all actuators (global feedback).

$$2)\ K = \begin{pmatrix} 12.21 & 0 \\ 0 & 2.35 \end{pmatrix} \text{N·s/m},\ \eta = 98.0\%,$$

i.e., each sensor signal is fed back locally to the colocated actuator (axial feedback).

$$3)\ K = \begin{pmatrix} 0 & 11.36 \\ -11.38 & 0 \end{pmatrix} \text{N·s/m},\ \eta = 2.6\%,$$

i.e., the sensor signal at position 1 is fed back to the actuator at position 2 and vice versa.

Table 5 Optimal parameters of one actuator/sensor configuration (dislocated)

Mode No.	ξ (actuator)	ξ (sensor)	k_{11}, Ns/m	η, %
1	0.2	0.2	50.0	99.7
2	0.317	0.343	18.72	89.3
3	0.429	0.463	16.59	93.5
4	0.591	0.614	14.31	92.4
5	0.695	0.702	12.57	84.3
6	0.772	0.776	10.14	85.7
7	0.825	0.835	10.47	91.3
8	0.898	0.901	10.63	76.5
9	1.0	1.0	3.96	79.1

Since in all three feedback schemes K is non-negative definite, the five-mode closed-loop system is asymptotically stable. Evidently, axial feedback gives the largest efficiency with low feedback gains that resemble the equivalent gains in the one actuator/sensor case (Table 2) for both positions. Contrarily, feedback scheme 3 produces an extremely low efficiency factor but with comparatively high gain factors. Moreover, regarding the evaluation model with 10 modes, spillover is predicted and observed experimentally for mode 7 with a frequency of 11.4 Hz. Figure 11 presents the corresponding time histories.

An important result is that a configuration of two actuators and two sensors can be more efficient than a configuration of only one actuator and one sensor, but this depends on the selected feedback strategy. Nevertheless, even overall sensor information (global feedback) may not be as useful as in axial feedback when comparing the amount of dissipated energy.

Conclusions

A flexible beam experiment has been constructed in order to demonstrate and verify advanced control laws based on direct velocity feedback. The new actuating and sensing system is based on an electrodynamic force actuator and an electro-optical displacement transducer that revealed almost ideal performance. This allowed the investigation of the interaction of controller/structure without the impact of hardware constraints. The structural dynamics of the gravity-loaded beam could be modeled with good accuracy, being an essential input for the controller design. Detailed studies on colocated and noncolocated one actuator/sensor positions favored the colocated configuration, since noncolocation proved to produce spillover due to the higher modes not being implemented in the design model or, potentially, even in the evaluation model.

By realization of a two actuator/sensor controller, better closed-loop behavior could be achieved: the amount of dissipated energy was increased when applying special feedback strategies (global or axial feedback), but global (rather than axial) feedback did not essentially improve the controller performance. For investigation of the closed-loop system dynamics, the experimental determination of complex eigenvalues by means of transfer functions proved to be most practicable. Only in cases of highly damped modes were the eigenvalues determined with poor accuracy. In all of the studies performed, no remarkable difference between the experimental results and theoretical predictions could be exhibited.

Future work will be directed toward the digital realization of controller feedback. Further studies are in preparation involving structures with frequency spectrums that include the closely spaced mode shapes (plates) more typical of large advanced space structures.

Acknowledgments

Experimental investigations require much team effort. Hence all members of the group on Satellite Dynamics deserve recognition. Many thanks to Dr. G. Schulz who made his optimization routines available to the authors.

References

[1]Balas, M. J., "Trends in Large Space Structure Control Theory: Fondest Hopes, Wildest Dreams," *IEEE Transactions on Automatic Control*, Vol. 27, 1982, pp. 522-535.

[2]Aubrun, J.-N., Ratner, M. J., and Lyons, M. G., "Structural Control for a Circular Plate," Lockheed Palo Alto Research Lab., 1983.

[3]Herrick, D., Canavin, J., and Strunce, R., "An Experimental Research of Modern Modal Control," AIAA Paper 79-0199, Jan. 1979.

[4]Schaechter, D. B., "Hardware Demonstration of Flexible Beam Control," AIAA Paper 80-1794, Aug. 1980.

[5]Montgomery, R. C., Horner, G. C., and Cole, S. R., "Experimental Research on Structural Dynamics and Control," *NASA Conference on Structural Dynamics and Control of Large Space Structures*, NASA Pub. 2187, Oct. 1980.

[6]Balas, M. J., "Direct Velocity Feedback Control of Large Space Structures," *Journal of Guidance and Control*, Vol. 2, 1979, pp. 252-253.

[7]Schulz, G. and Heimbold, H., "Integrated Actuator/Sensor Positioning and Feedback Design for Large Flexible Structures," AIAA Paper 82-1590, Aug. 1982.

[8]Schäfer, B. E., "Free Vibrations of a Gravity-loaded Clamped-free Beam," *Ingenieur-Archiv*, Vol. 55, 1985, pp. 66-80.

[9]Collatz, L., *Eigenwertaufgaben mit technischen Anwendungen*, Akademische Verlagsgesellschaft, Leipzig, 1949.

[10]Szabo, I., *Einführung in die Technische Mechanik*, Springer Verlag, Berlin, 1961.

[11]Holzach, H. and Lange, Th., "Development of an Electromagnetical Force Actuator System for Active Vibration Control," DFVLR, Oberpfaffenhofen, FRG, Tech. Note TN-1/84, 1984.